International Journal of Adhesion & Adhesives 60 (2015) 31–46

Contents lists available at ScienceDirect

International Journal of Adhesion & Adhesives

journal homepage: www.elsevier.com/locate/ijadhadh

FE simulation of the curing behavior of the epoxy adhesive Hysol EA-9321

O. Devaux [a,b], R. Créac'hcadec [a,*], J.Y. Cognard [a], K. Mathis [b], F. Lavelle [b]

[a] Laboratoire Brestois de Mécanique et des Systèmes EA4325, ENSTA Bretagne/ Université de Brest /ENIB/UEB, ENSTA Bretagne, 2 rue F. Verny, 29806 Brest Cedex 9, France

[b] CNES, 52 rue Jacques Hillairet, 75012 Paris, France

ARTICLE INFO

Article history:
Accepted 25 February 2015
Available online 18 March 2015

Keywords:
Adhesively-bonded joints
Curing degree
Thermal analysis

ABSTRACT

Cold-curing adhesives, characterized by an unsteady curing degree, present various advantages for assembling large scale structures set up under outdoor conditions. Thus various applications can be found in aerospace and automotive industries where structures are affected by thermal and mechanical loads. Hence, the curing state of the adhesive must be known to evaluate the lifetime of such bonded structures. The evolution of the polymerization of the adhesive Hysol EA-9321 during the curing process was examined in this paper. To that end, the curing degree of the adhesive was experimentally and analytically investigated for different curing cycles with a view to a potential application in the aerospace domain, where structures are assembled at low temperatures. Existing dynamic and isothermal curing models were applied to simulate the curing behavior of the adhesive. Then, an FEM model was developed to simulate the process of adhesive curing by taking into account a thermo-kinetic coupling.

1. Introduction

Structural adhesive bonding is well-established in the aerospace, automotive and aircraft industries. In this study, we will focus on the application of structural adhesives in the aerospace industry. Here, epoxy adhesives are used in the assembly stage of large scale structures, for instance on the bonded structure of Ariane 5 SYLDA, in addition to more conservative assembling methods such as bolting or riveting. This adhesive enabled the launcher to carry a second satellite inside the fairing. Due to its size, structures were erected and set up under outdoor conditions and the use of cold-curing adhesives, such as the adhesive Hysol EA-9321 [1], was one alternative for controlling the curing process. These kinds of epoxy adhesives are sensitive to their curing environmental conditions. Low-temperature curing leads to incompletely cured systems and therefore the development of full physical and mechanical properties is greatly decelerated. The mechanical properties of a cold-curing adhesive depend on the curing degree achieved at the end of the curing process. Thus, the determination of the curing cycle is one of the important factors to be considered in order to predict the lifetime of such bonded structures.

The curing process of a cold-curing adhesive such as Hysol EA-9321 is analyzed by solving the energy equation [2]:

$$\rho C_p \frac{\partial T}{\partial t} = \nabla(\lambda \nabla T) + \varphi_r \quad , \quad with \quad \varphi_r = \rho \Delta H_r \frac{\partial \alpha}{\partial t} \tag{1}$$

where ρ is the density of the adhesive, C_p the specific heat, λ the conductivity of the adhesive, T the temperature, H_r the total heat of the polymerization reaction and α is the degree of cure. Φ_r is the heat flux produced by the polymerization reaction.

There are several models to describe the change in thermal properties over the curing. Regarding the specific heat capacity, an approach comes from Balvers [3], who defined the specific heat capacity by a hyperbolic function depending on the temperature and on the glass transition temperature. A second approach was found by Johnston et al. [4] and defined that in the solid phase the heat capacity is only dependent on temperature. In the rubbery phase, the behavior is also dependent on the curing degree. A third approach used a rule of mixture definition [5–7]. In the same way, there are several approaches to predict thermal conductivity. Skordos et al. [8] defined it as a polynomial function of temperature and curing degree. Chern et al. [9] defined the thermal conductivity by a temperature dependent fourth order polynomial. Another approach consists in using a simple rule of mixture [10,11]. In this paper, the modification of the specific heat and thermal conductivity during curing was described by considering the chemical blend as a perfect mixture of resin and hardener weighted by the curing state α [10,11], i.e according to a simple rule of mixtures, as shown in Eqs. (2) and (3) [5–7]. The validity of this assumption will be discussed later in the paper. There are some ways to quantify these material properties. The specific heat capacity can be experimentally determined, using a Differential Scanning Calorimetry (DSC) analysis, by comparing the heat flow released by the sample to those of a calibration standard of known specific heat [11]. The thermal conductivity is investigated through the Transient

* Corresponding author. Tel.: +33 2 98 34 87 65; fax: +33 2 98 34 87 30.
E-mail address: Romain.Creachcadec@ensta-bretagne.fr (R. Créac'hcadec).

http://dx.doi.org/10.1016/j.ijadhadh.2015.03.005
0143-7496/

Plane Source method (TPS) [5,6,11,12].

$$C_p(\alpha,T)=(1-\alpha)C_p(0,T)+\alpha C_p(\alpha_{max},T) \quad (2)$$

$$\lambda(\alpha,T)=(1-\alpha)\lambda(0,T)+\alpha\lambda(\alpha_{max},T) \quad (3)$$

By considering the energy equation, it appears that the curing degree is a key parameter for the curing process study.

Generally, improvement of the adhesive properties depends on the formation of the cross linked molecular network, which is often influenced by the mechanisms and the kinetics of various chemical reactions. Therefore, understanding the curing process of the adhesive is essential in order to obtain better control of the cure reactions and consequently to optimize the properties of the final form of the adhesive.

In a bonded assembly, a non-linear increase in internal temperature profiles is induced by the exothermic chemical reaction and the amount of heating power supplied to the assembly structures. Hence, non-uniform curing leads to an incomplete cure and may affect adhesive properties. Thus, FE simulations are investigated to predict the temperature distribution and cure behavior of the adhesive Hysol EA-9321 in any location of the bonded area

During the curing process, the curing degree and the glass transition temperature evolve in the same way as the crosslinking progresses. The glass transition of the adhesive increases until a temperature at which the system reaches a glassy state and vitrifies. This process is dependent on curing temperature and curing time [13,14]. At low temperature (below the glass transition), the development of the glass transition temperature is slowed and achieves a low value: this reaction is diffusion controlled. In this paper, analysis is made at low curing temperature, i.e. under the glass transition temperature.

2. Kinetic analysis of the adhesive Hysol EA-9321

2.1. Material, experimental setup and curing conditions

The material object of this study was Hysol EA-9321 adhesive from Henkel, a two component thixotropic, solvent-free epoxy based resin. The adhesive is prepared using a mixing ratio of 2:1 by weight of the respective constituents (resin and hardener). According to the manufacturer's data sheets, a specimen cured for 1 h at 82 °C is completely cured (curing degree $\alpha=1$). The glass transition corresponding to this cycle is 109 °C. In addition, the manufacturer specifies a glass transition temperature of 88 °C for specimens cured for 5–7 days at 25 °C. A kinetic analysis such as the one presented in Section 2.2 for an isothermal temperature of 25 °C gives a curing degree of 0.4.

The heat released during the curing reaction was detected by using a heat-flux differential scanning calorimeter (DSC 20 Mettler TOLEDO TA3000) [15] connected to a thermal analyzer. This calorimeter is made of two steel pans. One of these is empty and the other contains a sample weighing between 5 and 10 mg.

At first, dynamic and isothermal scans were carried out to determine the kinetic parameters of each one. Then, both kinds of scans were conducted to simulate a few steps curing cycles.

Dynamic scans were led in the temperature range of 25–200 °C at constant heating rates of 5, 10, 15 and 20 °C/min. Isothermal scans were run at temperatures ranging from 25 to 100 °C. Equilibrium at the target isothermal temperature was reached in the sample holder with a rate of 20 °C/min. This rate was chosen as sufficiently fast to prevent the reaction between resin and hardener before the start of the isothermal scan. Coupled scans were made in the same way as previously, i.e. a dynamic scan was conducted until the required isothermal temperature, and then a second dynamic scan was conducted until the second required isothermal temperature.

For each scan, a second heating run on the same sample under the same conditions was carried out in order to define the baseline along which the curve heat flow vs. time is integrated.

2.2. Kinetic analysis of experimental results

The DSC curves in dynamic analysis are shown in Fig. 1. The shape of the exotherm was heating dependent. The value of the total heat released was determined by integrating heat flow vs. time under the exotherm. This heat of reaction ΔH_T, was independent of the heating rate (Table 1).

Fig. 2 shows the curing rate vs. time for isothermal scans. The maximum heat flow is reached faster for high curing temperatures, due to the acceleration of the reaction between resin and hardener. Table 2 presents the heat of reaction released during isothermal scanning. ΔH_{ISO} is calculated by integrating the area under the heat flow vs. time curves, defined as previously.

The heat flux measured by the DSC-system can be written in terms of enthalpy as:

$$\Phi=\left(\frac{dH}{dt}\right)_t \quad (4)$$

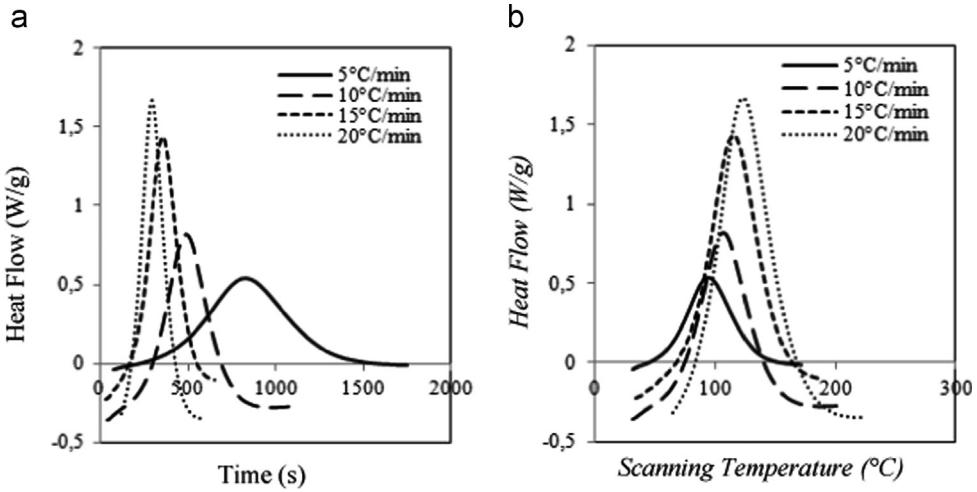

Fig. 1. Dynamic scanning: heat flow at different heating rates as function of (a) time and (b) temperature.

The application of Eq. (1), results in:

$$\frac{d\alpha}{dt} = \frac{1}{\Delta H_T}\left(\frac{dH}{dt}\right)_t \tag{5}$$

where ΔH_T is the total heat of reaction calculated during dynamic scans and $(dH/dt)_t$, the heat flow at time t measured by DSC isothermal scans. Hence, the curing degree α can be written as follows:

$$\alpha = \frac{\Delta H_t}{\Delta H_T}, \quad \text{with} \quad \Delta H_t = \int_0^t \left(\frac{dH}{dt}\right)_t \tag{6}$$

where ΔHt is the heat of reaction released during isothermal scan at time t.

In this way, intermediate curing states of the adhesive as a function of time over isothermal temperatures were determined. This is plotted in Fig. 3.

For each isothermal temperature, the curing degree increases until a plateau. At high temperatures, the plateau is reached after few minutes: 100% curing requires 46 min at 82 °C. At low temperature curing, the plateau is delayed: 38% is attained after 4 h and 25 min at 35 °C. Higher temperatures accelerate the reaction between resin and hardener. Hence, the plateau is quickly reached for high-curing temperatures.

2.3. Kinetic modeling and discussion

The curing kinetics could be approached in two ways: either phenomenological [16] or mechanistic models [17–19]. Phenomenological models are based on an empirical relation between reaction kinetics. The mechanistic approach was made from the balance of reactive species involved in the chemical reaction. Since the chemical composition of the adhesive constituents is unknown, phenomenological models were preferred to study the cure kinetics of the adhesive. These models were based on dynamic and isothermal approaches. The former describes the curing for a non-zero curing rate whereas the latter is used for isothermal loadings. Hence, both issues need to be investigated to predict properly any curing cycle which is a combination of dynamic and isothermal scans.

2.3.1. Dynamic modeling

An empirical model relating the curing rate, $d\alpha/dt$, to a function of the curing degree, α, for epoxies has the following expression:

$$\frac{d\alpha}{dt} = kf(\alpha) \tag{7}$$

where k is the time-dependent reaction rate, following Arrhenius law [20]:

$$k = Ae^{-\frac{E_a}{RT}} \tag{8}$$

where A (s^{-1}) is the pre-exponential factor, E_a (J/mol) is the activation energy, R (8.314 J/mol K) is the universal gas constant and T (K) the temperature.

According to the previous curves, an autocatalytic model was suggested [21]:

$$f(\alpha) = \alpha^m(1-\alpha)^n \tag{9}$$

where n and m are the reaction orders.

The kinetic parameters E_a, A, m and n were determined by fitting the experimental results to the autocatalytic model with the Kissinger [22] and Ozawa [23] methods.

A similar definition of the curing rate was obtained by defining a modified pre-exponential factor as:

$$A_f = C_f.A = C_f.\frac{e^K\left(\frac{d\alpha}{dT}\right)_p}{\alpha_p{}^m(1-\alpha_p)^n} \tag{10}$$

where C_f is the correction factor of A, K a parameter coming from the Kissinger method [19]. The terms $(d\alpha/dT)_p$ and α_p are the derivative of degree of cure to temperature and curing degree at the exothermic peak, respectively. Substituting k in Eq. (7) by Eqs. (8) and (9) and A_f in Eq. (8) by Eq. (10) results in the rate

Table 1
Total heat of reaction at different heating rates.

Parameter	dT/dt (°C/min)			
	5	10	15	20
ΔH_T (J/g)	334.1	351.03	326.66	353.1

Table 2
Isothermal scanning results.

Parameter	T_{cure} (°C)				
	35	45	60	70	82
ΔH_{ISO} (J/g)	130.73	202.07	240.03	310.03	341.18
α (–)	0.38	0.59	0.70	0.91	1.0
t	4h25	3h33	2h40	1h30	46 min

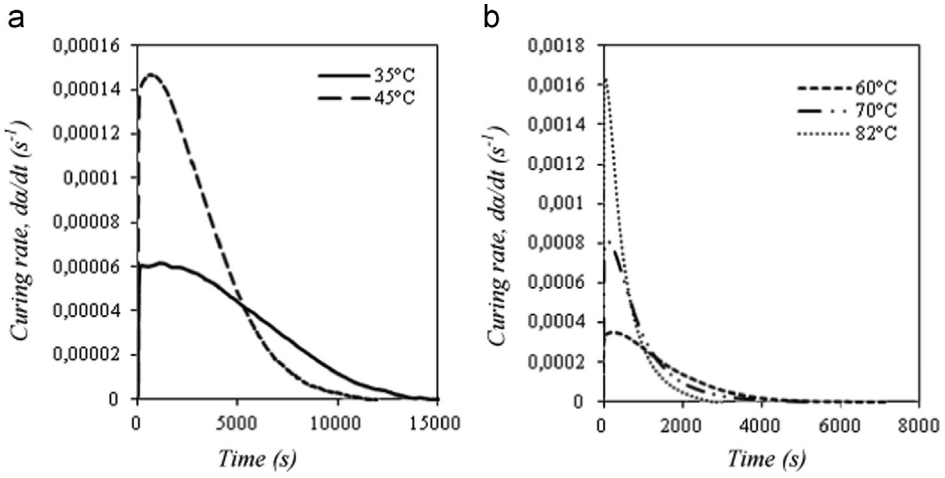

Fig. 2. Curing rate at different isothermal temperatures: (a) low-curing temperatures and (b) high-curing temperatures.

equation:

$$\frac{d\alpha}{dt} = C_f \cdot \frac{e^{K\left(\frac{d\alpha}{dT}\right)_p}}{{\alpha_p}^m (1-\alpha_p)^n} \cdot e^{-\frac{E_a}{RT}} \cdot \alpha^m (1-\alpha)^n \quad (11)$$

For both models, a non-linear least-square regression based on the Levenberg–Marquardt algorithm [24] was used to determine the parameters m, n and C_f. Table 3 shows its estimation. Then, Eq. (11) is numerically solved by using the fourth-order Runge–Kutta method [25]. A time-step size of 1 s was used to reach numerical convergence.

Fig. 4 shows the results for the different heating rates for both models. The curves predicted by both models also correlate the experimental results. However, in Fig. 4(a), curves predicted by the modified autocatalytic model in the peak area are closer to experimental results. Hence, the modified autocatalytic model is preferred to model dynamic scans because of its reliability and its accuracy compared to the empirical model.

2.3.2. Isothermal modeling

The isothermal curing behavior of an adhesive is written as a function of its curing degree:

$$\frac{d\alpha}{dt} = g(\alpha) \quad (12)$$

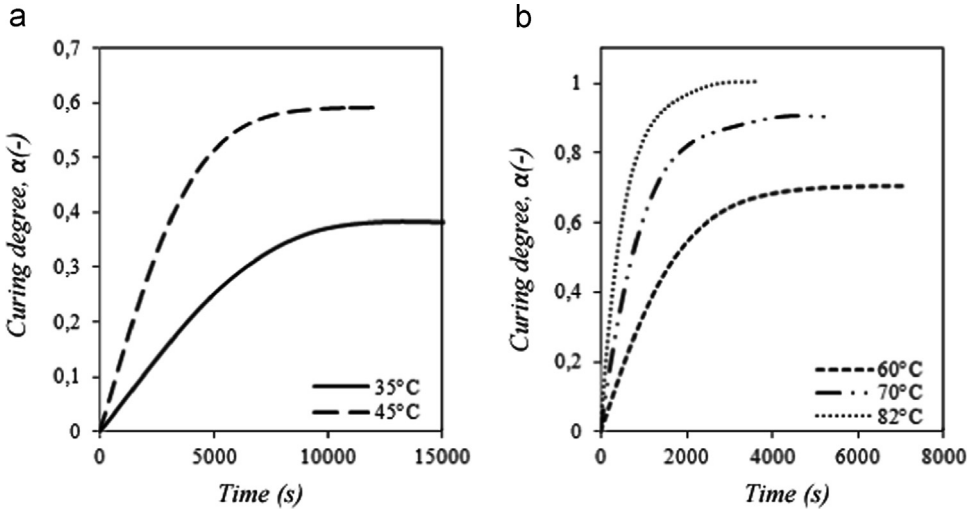

Fig. 3. Curing degree vs. time for isothermal temperatures.

Table 3
Kinetic parameters from a dynamic model.

Model	Parameter	dT/dt (°C/min)			
		5	10	15	20
Kissinger and Ozawa	Ea (kJ/mol)	60.03	60.03	60.03	60.03
	A (s^{-1})	1.77×10^6	1.77×10^6	1.77×10^6	1.77×10^6
	m	0.16	0.21	0.23	0.29
	n	1.54	1.51	1.41	1.63
Modified model	C_f	0.97	1.06	1.05	0.98

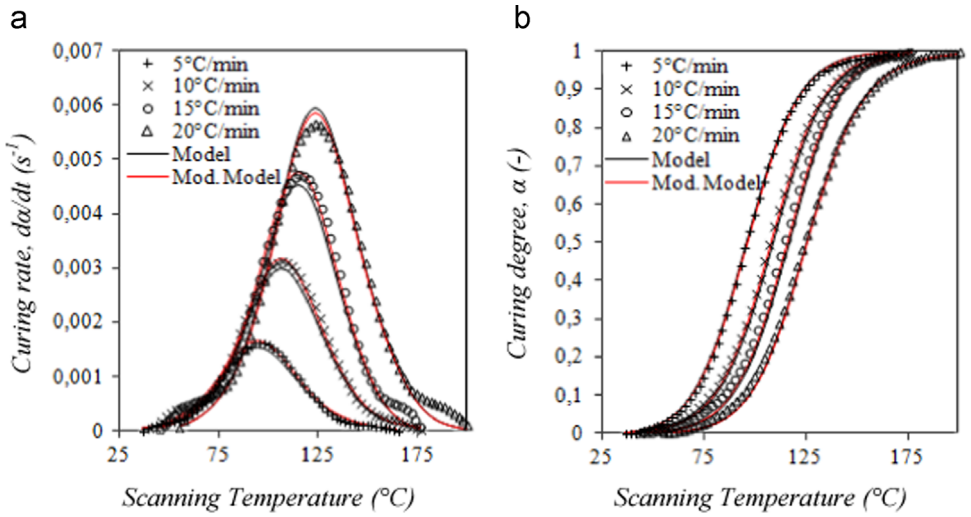

Fig. 4. Comparison of experimental and autocatalytic model results: (a) curing rate vs. temperature and (b) curing degree vs. temperature.

Some models were used to describe this process. The simplest model corresponds to an n-th order kinetic expression as follows:

$$g(\alpha) = k(1-\alpha)^n \tag{13}$$

where n is the reaction order and k, the rate constant given by Arrhenius law defined previously.

Another kinetic expression was proposed by Horie [26] as the following equation:

$$g(\alpha) = (k_1 + k_2\alpha)(1-\alpha)^2 \tag{14}$$

where k_1 and k_2 are the kinetic rate constants:

$$k_i = A_i e^{-\frac{E_{a_i}}{RT}} \qquad i = 1,2 \tag{15}$$

where A_i (s^{-1}) is the pre-exponential factor, E_{ai} (J/mol) is the activation energy, R (8.314 J/mol K) is the universal gas constant and T (K) the temperature.

Kamal and Sourour [27,28] extended the previous model using two additional empirical power law exponents m and n in addition to the constants k_1 and k_2. Thus, Eq. (14) becomes:

$$g(\alpha) = (k_1 + k_2\alpha^m)(1-\alpha)^n \tag{16}$$

Approaching the glass transition temperature, the chains formed induced a decrease in the movement of the reactive species. In such cases, the reaction rate was decelerated and the further reaction became diffusion controlled. To take into account this phenomenon, Chern and Phoehlein [29] proposed another definition of the reaction rate by adding a diffusion factor to the kinetic model $g(\alpha)$:

$$\left[\frac{d\alpha}{dt}\right]_{diffusion} = g(\alpha).\frac{1}{1+e^{C(\alpha-\alpha_c)}} \tag{17}$$

where $(1/1+e^{C(\alpha-\alpha_c)})$ is the diffusion control factor, C is an empirical constant which is temperature dependent and α_c is the critical curing degree at which diffusion initiates. $g(\alpha)$ is the kinetic expression of the previous models.

In order to evaluate the kinetic parameters appearing in each equation, the following procedure was followed. At first, the diffusion-controlled phenomena was ignored in order to determine which kinetic model best described the curing process of the adhesive. The parameters were determined using a non-linear least square regression analysis [23] and each curing rate equation was solved with the fourth-order Runge–Kutta method [24]. Then, kinetic parameters of the chosen model were determined by taking the diffusion into account. On one hand, the initial parameters and the diffusion parameters were defined separately by using two non-linear least square regressions. On the other hand, the parameters were determined using only one regression. The first method was preferred because of accuracy of the results. For all simulations, the time step taken was sufficiently small (time step of 1 s) to reach the Runge Kutta-method convergence.

Figs. 5 and 6 show the results for the three models defined previously without taking into account the diffusion phenomenon. The modeling curve using the Kamal and Sourour model correlates well with the experimental curves compared to those of the other models.

In Figs. 5(b) and 6(b), a critical value of the curing degree appears with which the experiment and Kamal and Sourour model no longer correlate. This gap is due to the diffusion phenomenon. For low curing temperature, this degree of cure is reached at 40% for 35 °C and around 60% for 45 °C. Regarding high curing temperature, the value is 70% for 60 °C, 90% for 70 °C and 100% for 82 °C. From there, simulations were made by taking into account the Kamal and Sourour model by adding the diffusion term:

$$\left[\frac{d\alpha}{dt}\right]_{\substack{K\&S \\ Diffusion}} = (k_1 + k_2\alpha^m)(1-\alpha)^n.\frac{1}{1+e^{C(\alpha-\alpha_c)}} \tag{18}$$

Figs. 7 and 8 show the correlation between experimental and simulation curves. The simulation curves were based on the Kamal and Sourour model with and without diffusion. The difference between these models is primarily seen on the curing degree vs. time curves (Figs. 7(b) and 8(b)). In the late stage of curing reaction, the effect of diffusion on the curing rate is apparent, especially at low isothermal curing temperatures. The isothermal maximum degree of cure goes from 0.55 to 0.38 for a curing temperature of 35 °C and from 0.7 to 0.6 for a curing temperature of 45 °C (Fig. 7(b)). It ranges from 0.86 to 0.70 for an isothermal temperature of 60 °C, from 0.95 to 0.92 for an isothermal temperature of 70 °C. Experimental results were accurately simulated by the Kamal and Sourour model with diffusion.

Table 4 shows the kinetic parameters identified with the non-linear least square regression analysis. The values of several parameters can be related to the temperature. The rate constants k_1 and k_2 increase with the curing temperature. These quantities are related to the temperature using Arrhenius law (Eq. (15)). The reaction order n decreased with increased temperature. The critical curing degree increased with isothermal temperature. Thus, the curing behavior of the adhesive Hysol EA-9321 depends only on the temperature.

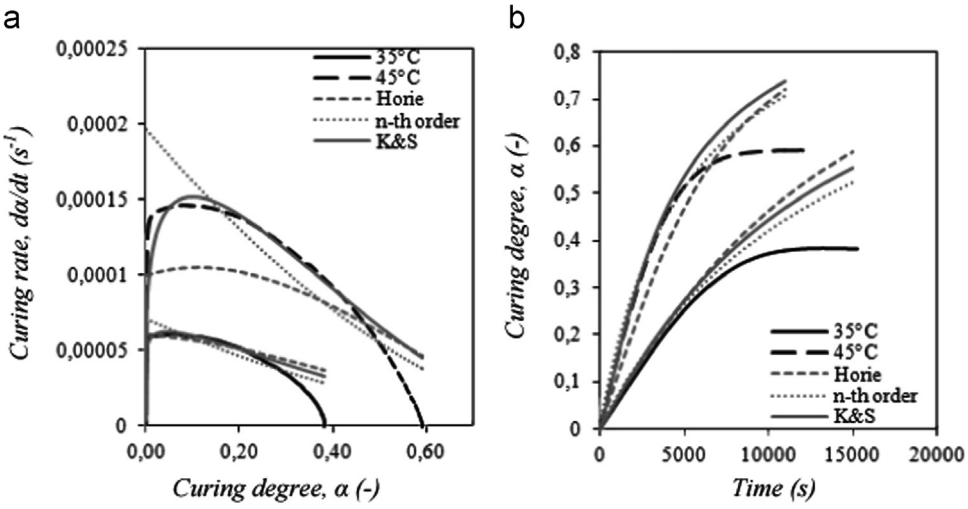

Fig. 5. Comparison of experimental and isothermal model results for low-curing temperature: (a) curing rate vs. curing degree and (b) curing degree vs. time.

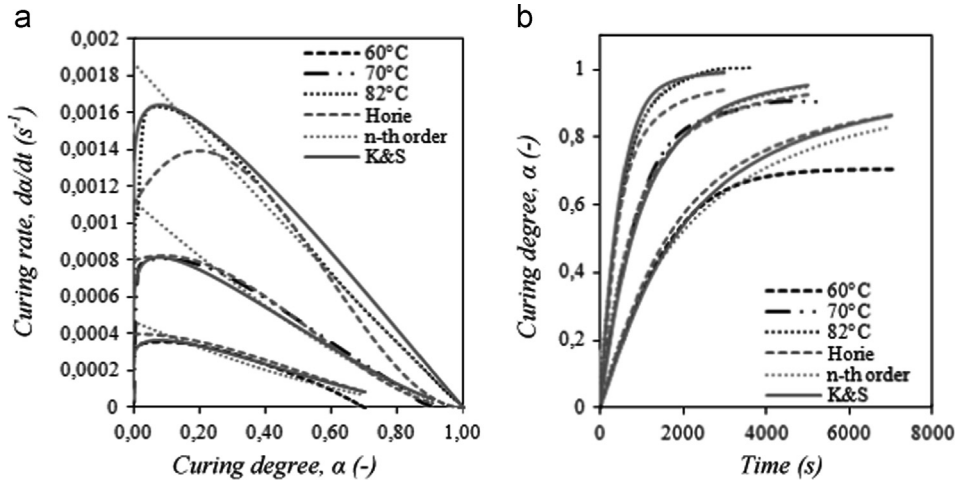

Fig. 6. Comparison of experimental and isothermal model results for high-curing temperature: (a) curing rate vs. curing degree and (b) curing degree vs. time.

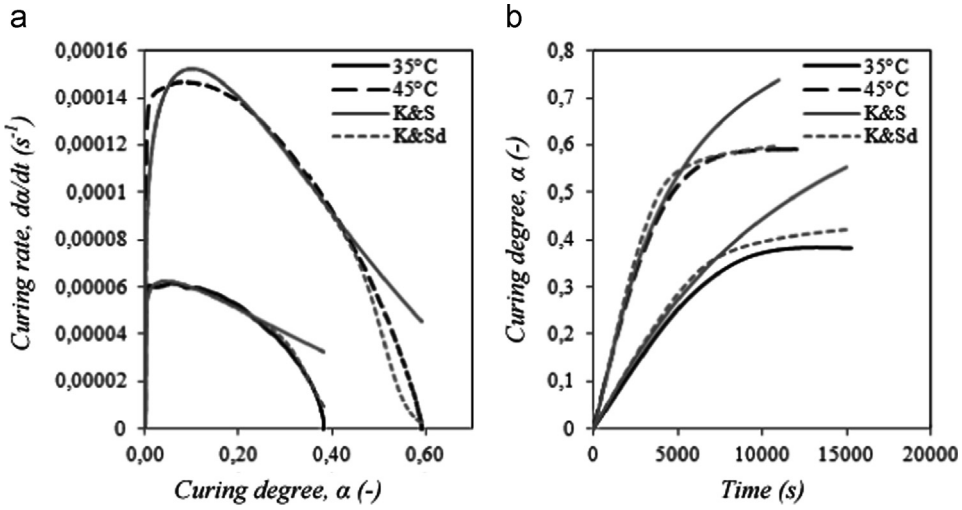

Fig. 7. Comparison of experimental and isothermal model results with diffusion for low-curing temperature: (a) curing rate vs. curing degree and (b) curing degree vs. time.

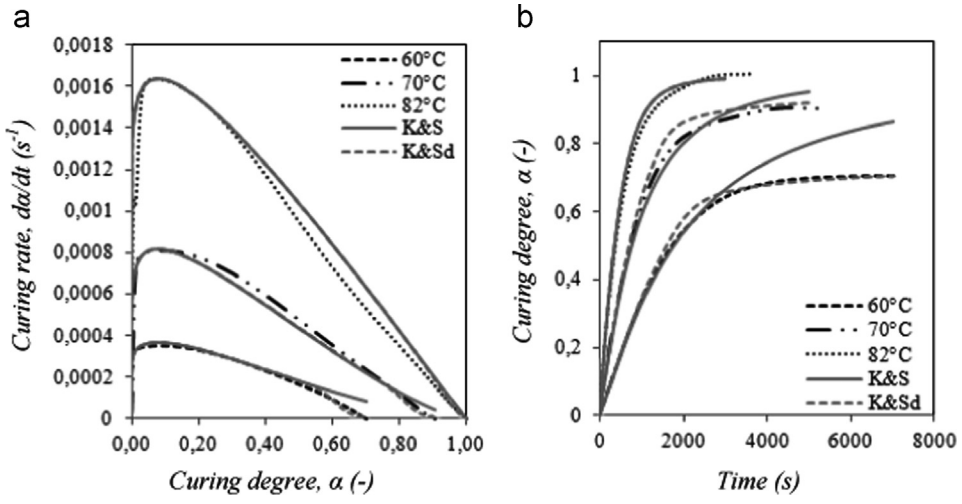

Fig. 8. Comparison of experimental and isothermal model results with diffusion for high-curing temperature: (a) curing rate vs. curing degree and (b) curing degree vs. time.

2.3.3. Discussion

As previously studied, the curing behavior of the adhesive Hysol EA-9321 can be described through dynamic and isothermal approaches. Regarding the isothermal model, the curing behavior is temperature dependent. Hence, this model is known for a wide range of temperatures. Dynamic scans can be considered as a series of isothermal heating with a period of one second. Thus, we can assume that the isothermal model can be used to model dynamic heating.

In order to validate this assumption, experimental dynamic results were simulated with the isothermal model described previously. This model was modified to take into account the global behavior of the adhesive Hysol EA-9321, i.e at a series of isothermal temperatures. Table 5 shows the kinetic parameters used to model the dynamic scans. The parameters m and n were approximated by an average value independent of the temperature. The critical curing degree evolved linearly with temperature until the glass transition temperature.

Fig. 9 shows that the curves predicted by the isothermal model correlate well with those of experimental dynamic scans. The slight delay caused by the isothermal model (Fig. 9(b)) seems acceptable regarding the fast heating rates. The kinetic parameters identified and the consideration of dynamic scans as a series of isothermal temperatures are validated.

3. Finite element simulation of the polymerization of the adhesive Hysol EA-9321

Considering the kinetic analysis, the cure modeling of the adhesive Hysol EA-9321 may be considered as a transient heat-transfer analysis by taking into account the effect of the adhesive polymerization reaction. A numerical procedure was proposed and experimentally verified in this section.

3.1. Solution procedure

The problem can be classified into two categories. On one hand, it consists in a transient thermal analysis by solving the energy equation. On the other hand, an evolution law for the curing degree must be provided.

A procedure is proposed in which a general-purpose FE package is employed to perform transient heat-transfer analysis and programs are developed to simulate the cure reaction of the adhesive Hysol EA-9321. Fig. 10 provides the flow chart of the procedure.

The available pre-processor to the FE package is used to create the model and to generate the initial input data file for the analysis. Three user subroutines were developed to take into account problems generated by the adhesive curing. The subroutine SDVINI was used

Table 4
Kinetic parameters from isothermal Kamal and Sourour model with diffusion.

Model	Parameter	T (°C)				
		35	45	60	70	82
Kamal and Sourour	k_1 (s^{-1})	1.52×10^{-6}	7.48×10^{-6}	2.26×10^{-4}	2.38×10^{-5}	6.84×10^{-4}
	k_2 (s^{-1})	8.80×10^{-5}	2.18×10^{-4}	4.14×10^{-3}	1.21×10^{-3}	1.60×10^{-3}
	m	0.0905	0.12	0.311	0.13	0.15
	n	1.92	1.8363	1.63	1.38	1.04
Kamal and Sourour diffusion	C	38	38	38	38	38
	α_c	0.36	0.52	0.64	0.84	0.98

Table 5
Cure kinetic coefficients of the Hysol EA-9321 for the Kamal and Sourour model with diffusion.

Parameters							
m	n	A_1 (s^{-1})	A_2 (s^{-1})	E_1 (J/mol)	E_2 (J/mol)	C	α_c
0.16	1.56	6.6e−5	4.6e5	2000	6.0e4	38	$0.013\ T - 0.09\ T \leq T_g$ $0.97\ T > T_g$

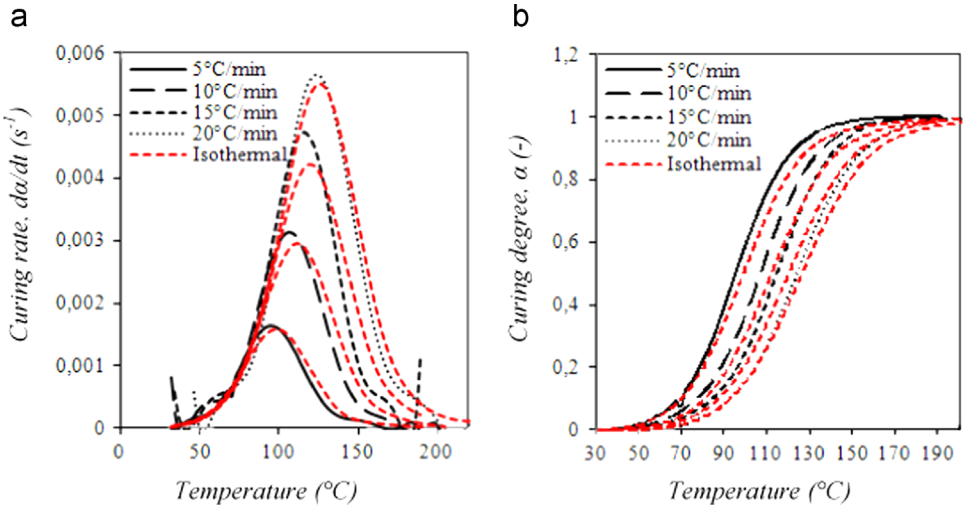

Fig. 9. Isothermal modeling of dynamic experimental data: (a) curing rate vs. temperature and (b) curing degree vs. temperature.

to define the initial values of specific heat $C_p(0,T)$ and conductivity $\lambda(0,T)$. These quantities were experimentally determined according to the procedure detailed in the next section. The subroutine HETVAL consisted in determining the heat produced at each Gauss point, by the reaction of polymerization and the curing degree by solving the cure kinetic equation of Kamal and Sourour with diffusion (Eq. (18)) with parameters validated in Section 2.3.3. As defined previously, specific heat and conductivity are related to temperature and curing degree. Hence, the subroutine USFLD enabled these material parameters to be updated at each increment.

3.2. Experiment

In order to validate the previous procedure and to test its reliability, the curing of an adhesive block was considered. Other experiments were performed simultaneously in order to determine values of specific heat and conductivity for uncured and totally cured adhesive.

3.2.1. Curing of a cylindrical block of adhesive

To determine curing degree evolutions of the adhesive Hysol EA-9321 under various curing time and temperature conditions, an experimental procedure was developed. The uncured adhesive was introduced into a steel tube ($h2=43$ mm, $e=1.2$ mm and $r=11.3$ mm). The tube was placed vertically on a steel plate ($h1=3$ mm) to prevent the adhesive from flowing out (Fig. 11).The whole was then kept in the oven for several curing cycles (1 h at 100 °C, 3 h at 60 °C). In order to verify the numerical modeling, temperature profiles inside the adhesive block were recorded throughout the experiment and compared with the numerical results. Fig. 11(b) illustrates the schematic diagram of the experimental set-up used to measure the temperature evolution during the curing process. The thermocouples were placed at different locations inside the adhesive, points A, B and C in Fig. 11(b), and connected to a data acquisition system to monitor the temperature vs. time.

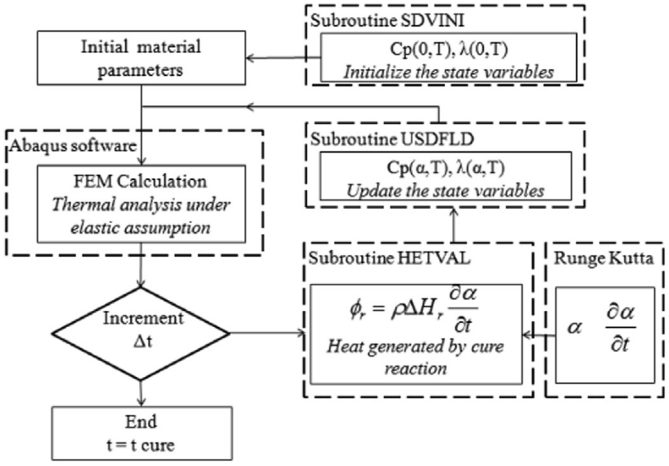

Fig. 10. Flow chart for FE procedure of curing process.

3.2.2. Determination of specific heat and conductivity

Determination of specific heat was accomplished by using Differential Scanning Calorimetry (DSC). These DSC experiments were carried out on a Perkin-Elmer DSC-7. The DSC heat flow signal from the adhesive Hysol EA-9321 was compared to the DSC signal of a calibration standard of known specific heat. Both curves were corrected by a baseline correction. This baseline correction was achieved by measuring heat flow released by an empty sample. Isothermally, the baseline indicated the differential losses of the two sample holders at the initial temperature. Determination of C_p according to ASTM E1269 [30] was determined by using a three step technique. The experiment was conducted with an empty sample crucible for baseline determination. Then, a measurement with a sapphire sample crucible was performed for calibration standard. Finally, heat flow was measured for a sample crucible of cured and uncured adhesive Hysol EA-9321. The same procedure was used for the four experiments: an isothermal scan was made for 10 min at 25 °C, a dynamic scan from 25 °C to 150 °C at a heating rate of 10 °C/min and an isothermal measurement for 10 min at 150 °C was performed.

To determine the specific heat capacity of the uncured adhesive, the previous procedure was applied directly to the resulting mixture of the resin and hardener. Concerning the heat capacity of the cured adhesive, a heating from 25 °C to 150 °C was performed before applying the previous procedure.

Fig. 12 shows results obtained after testing. Regarding the uncured adhesive, a change in the slope is observed. It corresponds to the glass transition temperature. The specific heat capacity of the uncured adhesive was the value calculated before this point.

The specific heats of cured and uncured adhesive were calculated as follows:

In a DSC cell, under the previous conditions, the heat flow measured on the sample side is expressed by the following heat transfer equation:

$$\left(\frac{dH(T)}{dt}\right)_{sample} - \left(\frac{dH(T)}{dt}\right)_{baseline} = m_{sample} C_{p,sample} \frac{dT_{sample}}{dt} \quad (19)$$

where $dH/dt(T)_{sample}$, $dH/dt(T)_{baseline}$ are the heat flow rates of sample (adhesive Hysol EA-9321), baseline. m_{sample} is the mass of the sample and T_{sample} the temperature of the sample.

Thus the experiment with the standard can be written in the same way:

$$\left(\frac{dH(T)}{dt}\right)_{standard} - \left(\frac{dH(T)}{dt}\right)_{baseline} = m_{standard} C_{p,standard} \frac{dT_{standard}}{dt} \quad (20)$$

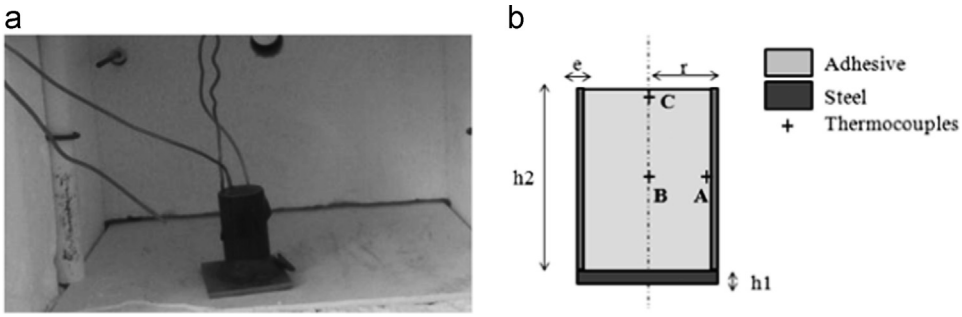

Fig. 11. (a) Experiment and (b) schematic diagram of the experimental set-up.

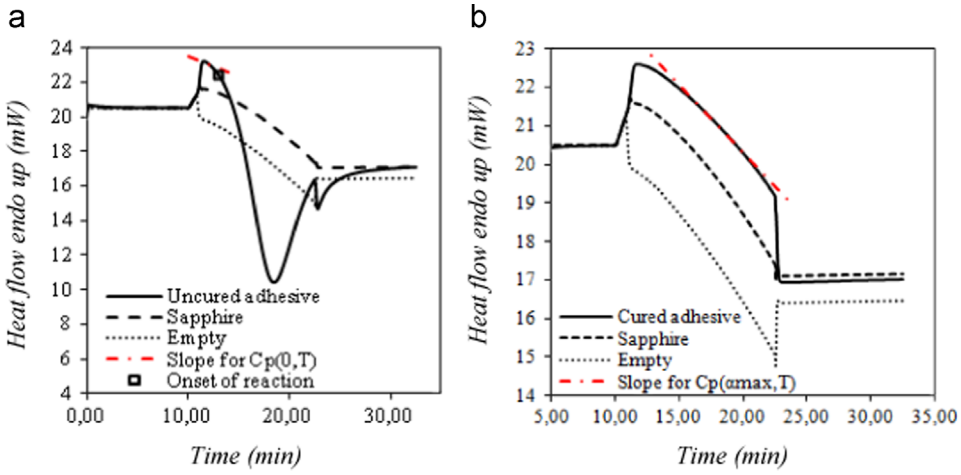

Fig. 12. Heat flow endo up vs. time: (a) uncured adhesive sample and (b) cured adhesive sample.

where $dH/dt(T)_{standard}$, $dH/dt(T)_{baseline}$ are the heat flow rates of reference (sapphire), baseline. $m_{standard}$ is the mass of the reference and $T_{standard}$ the temperature of the sample.

In the previous procedure, the sample and reference are submitted to the same temperature, hence the same heating rate. It can be deduced that

$$C_{p,sample} = \frac{m_{standard}}{m_{sample}} \frac{\frac{dH(T)}{dt}_{sample} - \frac{dH(T)}{dt}_{baseline}}{\frac{dH(T)}{dt}_{standard} - \frac{dH(T)}{dt}_{baseline}} . C_{p,standard} \quad (21)$$

$(dH(T)/dt_{sample})$ for the uncured and fully cured adhesive was chosen as detailed in Fig. 12(a) and (b). For the uncured adhesive, it is necessary to consider temperatures below the onset of the polymerization reaction (in our case, for temperatures under 45 °C). The previous kinetic analysis (Section 2.3.1) shows a value of curing degree below 0.1. It is not surprising since, in this area, the temperature goes from 25 to 40 °C at a heating rate of 10 °C/min. This rate is sufficiently high to prevent the adhesive from curing.

By applying Eq. (21), the specific heats of uncured and cured adhesive Hysol EA-9321 were related to the temperature as follows:

$$C_p(0,T) = 1.50 + 0.002T \quad \left(\mathrm{J\,g^{-1}\,{}^{\circ}C^{-1}}\right)$$

$$C_p(\alpha_{max},T) = 0.91 + 0.004T \quad \left(\mathrm{J\,g^{-1}\,{}^{\circ}C^{-1}}\right) \quad (22)$$

Thermal conductivities of uncured and cured adhesive were taken from a previous study.

$$\lambda(0,T) = 0.19 \quad \left(\mathrm{W\,m^{-1}\,K^{-1}}\right)$$

$$\lambda(\alpha_{max},T) = -2.73.10^{-4}T + 4.00.10^{-1} \quad \left(\mathrm{W\,m^{-1}\,K^{-1}}\right) \quad (23)$$

The orders of magnitude of specific heat capacity and thermal conductivity of uncured and cured adhesive are not surprising since the more the adhesive is cross linked, the easier it is to heat. Therefore, the specific heat decreases. The heat transfer is more important, thus, the thermal conductivity increases.

3.3. FE model

In order to understand the curing behavior of the previous experiment, a two-dimensional FE analysis on an axisymmetric slice was performed (Fig. 13) by using adequate boundary conditions. Due to the axial symmetry, the mesh was performed using an 8-node axisymmetric thermally coupled quadrilateral, biquadratic in displacement and bilinear in temperature (CAX8T elements of the Abaqus element library). A mesh with 6 elements in the x-direction and 40 elements in the y-direction was used for the adhesive. A step-time size of 1 s was used to predict accurate results. In this model, a film convection on the faces of the assembly exposed to the oven environment modeled the thermal loading, using a heat transfer coefficient characteristic of forced convective heating. Results are presented for steel plate and an elastic behavior was assumed for the adhesive Hysol EA-9321. Table 6 shows the material parameters used.

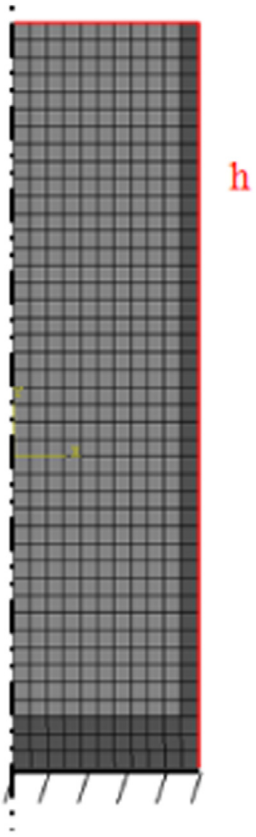

Fig. 13. Mesh and boundary conditions.

The FE procedure of curing process was firstly applied to one element (a 4-node plane strain thermally coupled quadrilateral, bilinear in displacement and temperature). A ramp from 25 °C to 200 °C at a heating rate of 10 °C/min was applied. Then, the curves curing-rate vs. temperature and curing degree vs. temperature were

compared with those predicted by the model of Kamal and Sourour with diffusion (Fig. 9). It appears that the curves predicted by the FE model correlate well with the curves of the model. This intermediate step was a way to validate the FE procedure.

After that, the temperature and the degree of cure of the adhesive during the curing were simulated by using the finite element model described previously. Then, the former were compared with experimental data. The simulated temperature and degree of cure were taken at the location of the thermocouple probes used in the experimental procedure. It was assumed that no thermal perturbation was generated by the thermocouple.

3.4. Results and discussion

3.4.1. Validity of the model

Fig. 14 shows the temperature and curing degree profiles for different curing cycles obtained by simulation and experiment in B location (Fig. 11(a)). The evolution of the curing degree for the experiment was obtained as follows:

Fig. 14(a) shows the temperature and curing degree profiles for different curing cycles obtained by simulation and experiment in B location (Fig. 11(a)). The evolution of the curing degree for numerical and experimental results was obtained from the evolution of the temperature inside the adhesive, as follows:

As shown previously in Section 2.3.3, a modified model of Kamal and Sourour with a dependence on temperature of some parameters was proposed. Hence, the parameters of this model were known for the temperature measured during the experiment and for the FEM numerical model Fig. 14. Then, Eq. (18) was solved using a fourth-order Runge–Kutta method. This depicted the evolution of the curing degree vs. time corresponding to the experimental and numerical temperatures of Fig. 14(a).

The predicted temperature and the curing degree of the adhesive for each curing cycle (60 °C and 100 °C) were in good agreement with the experimental results. Thus, the validity of the model was confirmed, as well as the values determined for kinetic and thermal parameters. Similar results are observed for locations in A and C (Fig. 11(a)).

There are few temperature and curing degree discrepancies between experimental and simulation results. These differences can firstly come from kinetic and thermal parameters. Secondly, they can be explained by the assumptions considered for the modeling. Furthermore, the adhesive thickness was supposed to be constant whereas in reality a shrinkage behavior due to the curing reaction and thermal expansion can be generated [31]. In addition, the thermocouples could be displaced from their initial position during the experiment.

A sensitivity analysis on thermocouple position, kinetic, thermal parameters and the adhesive thickness was performed to understand better the differences between experimental and simulation results.

Table 6
Material properties.

Material	Steel	Hysol EA-9321
Young's Modulus E [MPa]	210 000	2900
Poisson ν	0.3	0.36
Density ρ [kg m^{-3}]	7800	1250
Specific heat C_p [J kg^{-1} K^{-1}]	0.5	$C_p(0,T)=1.50+0.002\ T$ $C_p(\alpha_{max},T)=0.91+0.004\ T$
Conductivity λ [W m^{-1} K^{-1}]	25	$\lambda(0,T)=0.19$ $\lambda(\alpha_{max},T)=-2.73^{e-4}T+4.0^{e-1}$

3.4.2. Influence of the thermocouple location

The temperature in the adhesive was experimentally measured thanks to thermocouples. The latter were placed in the adhesive cylinder before the curing process. During the curing process, the adhesive passed from the raw (uncured liquid) to the cured rubbery and ultimately, to the cured glassy state. At the beginning of curing, the adhesive is an uncured liquid. Hence, the thermocouple positions may be affected by the adhesive state during curing.

The experiment was the same as before but the thermocouple was located in point D (Fig. 15) between points A and B (Fig. 11(a)) in order to show the influence to get closer to the side wall or to the middle of the tube. The temperature was experimentally measured and compared to results predicted by simulation. Then, the location of the thermocouple was used as a reference and the temperature and curing degree were numerically investigated around this reference.

Figs. 16 and 17 show the effect of vertical and horizontal displacement on the temperature and the curing degree profiles for a curing at 60 °C.

The temperature and the curing degree were not affected by a vertical displacement of the thermocouple (Fig. 17). However, radial displacements were important (Fig. 16). Regarding the temperature, the difference being essentially the change in the maximum value reached. For instance, a thermocouple which was 2 mm closer to the adhesive core from its initial position was responsible for an increase in maximum temperature of 13 °C. In the same way, a probe which was 4 mm from its first location caused a reduction of 17 °C in the peak temperature. This modification had repercussions on the curing

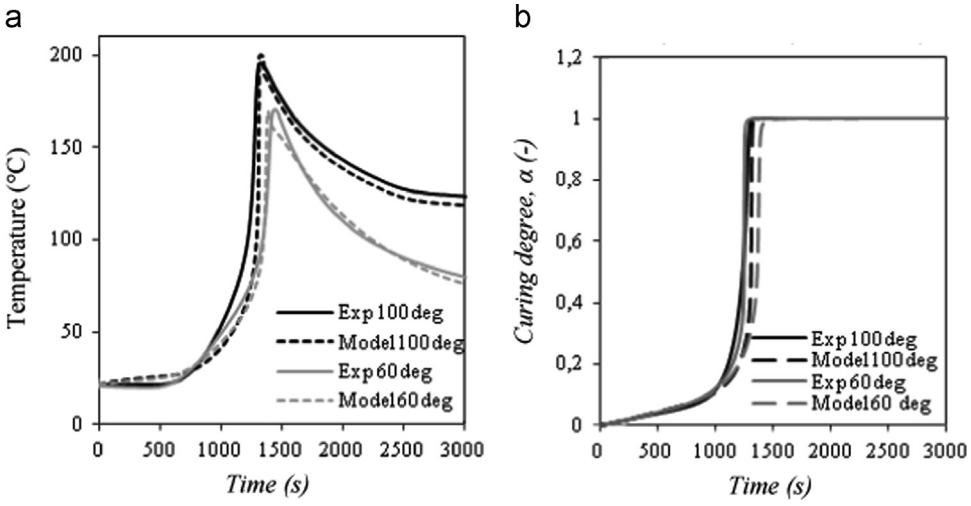

Fig. 14. Comparison of experimental and predicted results: (a) temperature-time history and (b) curing degree-time history.

degree (Fig. 16(b)). It is not surprising, since the thermal conductivity is lower for the steel tube than the adhesive. Thus, the difference with the temperature applied on external surfaces of the tube is greater in the adhesive core than close to the side wall. Indeed, a change in the maximum temperature delayed or accelerated the maximum value reached by the curing degree. The curing degree reached its maximum after 1515 s for a probe 2 mm above the first position against a maximum obtained after 1366 s for a thermocouple below its initial position by 4 mm.

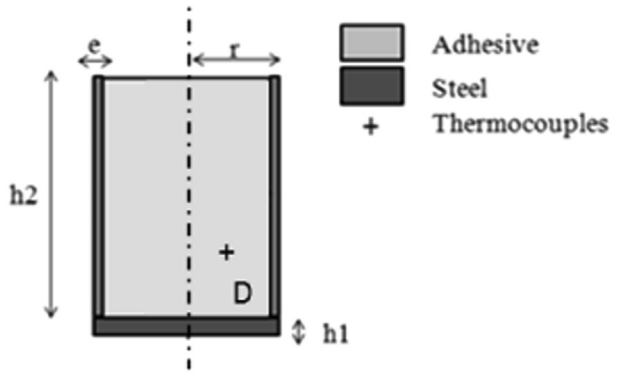

Fig. 15. Location of the thermocouple used for the sensitivity analysis of the thermocouple location.

3.4.3. *Influence of kinetic parameters*

The model used to describe the curing behavior of the adhesive Hysol EA-9321 (Section 2.3.3) came from the assumption that dynamic scans were a series of isothermal measurements. Hence, the parameters of this model were an average of parameters of each isothermal scan. This assumption caused a modification in the physical properties of input parameters of the kinetic problem and can affect the temperature and curing degree profiles resulting from the energy equation.

A parametric study was carried out on kinetic parameters such as total heat of reaction ΔH_T, reaction orders m, n, the activation energies E_1, E_2 and the rate constants k_1, k_2. For each simulation, a cure cycle of three hours at 60 °C was applied. The temperature and curing degree profiles were simulated at the location of a thermocouple used during experiments.

Fig. 18 shows the effect of the total cure enthalpy on the temperature and curing degree profile during curing. This parameter had an important impact on the predicted results, not only for the peak temperature but also for the slopes of these curves. A variation of 20% in the total heat of reaction resulted in a change of

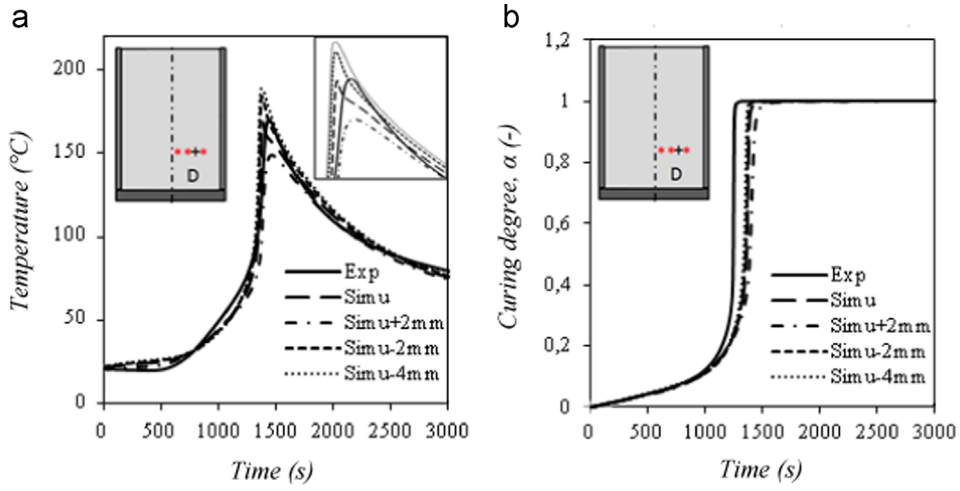

Fig. 16. Effect of the thermocouple location in the horizontal direction on (a) the temperature-time history and (b) the curing degree-time history at the point D(8;10) in the adhesive.

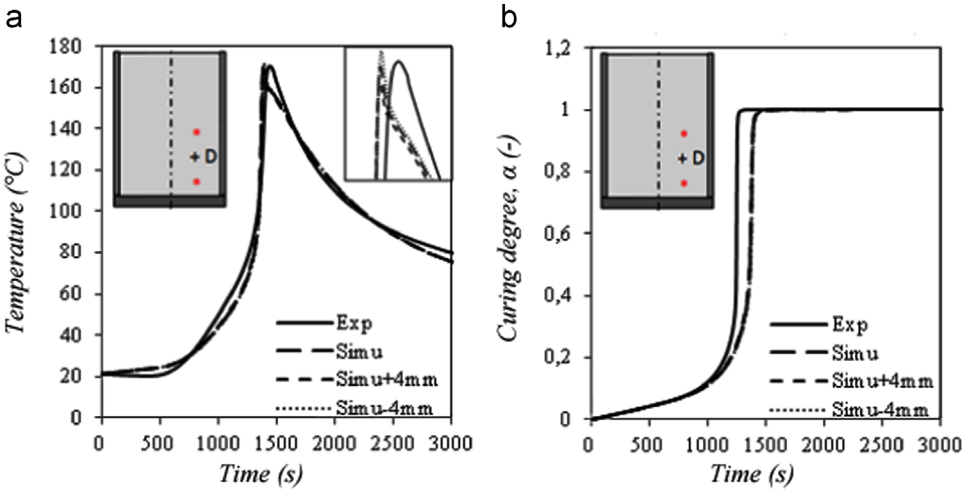

Fig. 17. Effect of the thermocouple location in the vertical direction on (a) the temperature-time history and (b) the curing degree-time history at the point D(8;10) in the adhesive.

about 32 °C in the peak temperature (Fig. 18(a)). Considering this, a modification in the cure enthalpy delayed or accelerated the time in which the maximum value of the curing degree was reached: a delay of 162 s for a 20% decrease in the enthalpy and an acceleration of 319 s for a 20% increase in the total heat of reaction.

The reaction order m and n have very few effects on the temperature and curing degree profiles (Figs. 19 and 20). In fact, a variation of 20% in the orders had no impact on the slopes of the curves and the maximum values reached.

Variations in the rate constants had different impacts on the simulation results (Figs. 21 and 22). Regarding the first rate constant A_1, a modification caused no effect on the temperature and curing degree responses. It was not surprising since, in Eq. (18), the first constant rate had no effect on the curing rate. It was just used to initialize its value. Contrary to the previous constant, the second rate constant affected the temperature and curing degree profiles (Fig. 22); the higher the rate constant, the faster the cure reaction. This was responsible for a higher slope in the temperature-time response corresponding to the highest value of the rate constant. It appeared once the reaction had taken, i.e. at around 60 °C. The state of cure was changed in time as shown in Fig. 22(b). About 1420 s were necessary to attain the maximum curing degree for an increase of 20% in the rate constant A_2 against 1563 s for the initial reaction rate and 1589 s for a decrease of 20% in the rate constant.

The effects of a variation in the activation energies E_1 and E_2 on the temperature-time and curing degree-time profiles appeared in Figs. 23 and 24. For the same reasons as for the rate constant A_1, Fig. 23 shows that the energy activation E_1 had no effect on the temperature and curing degree responses. Regarding the activation energy E_2, Fig. 24 shows that this activation caused a great impact on the simulation responses. The lower the activation energy, the faster the cure. Thus, the slopes of the temperature curves (Fig. 24(a)) were lower for the higher value of activation energy. Furthermore, an increase in the energy activation value E_2 increased the time necessary to obtain the maximum value of the curing degree. About 1420 s were necessary to attain the maximum curing degree for a decrease of 5% in the activation energy E_2 against 2269 s for the initial reaction rate and 936 s for an increase of 5% in the rate constant.

3.4.4. *Influence of thermal parameters*

Thermal parameters such as heat capacity and thermal conductivity were previously related to temperature and curing degree. Hence, these thermal parameters were also influenced by the modification of the physical properties of the input parameters. In the same way as previously, a sensitivity study on these parameters was carried out. A curing cycle of 60 °C was applied and the temperature at the place of a thermocouple was simulated.

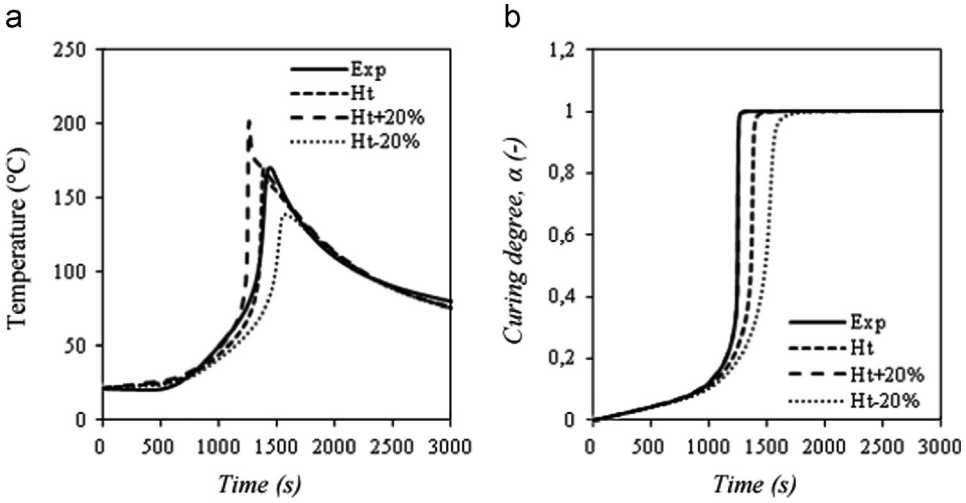

Fig. 18. Effect of the total heat of reaction on (a) the temperature-time history and (b) the curing degree-time history at the point D(8;10) in the adhesive.

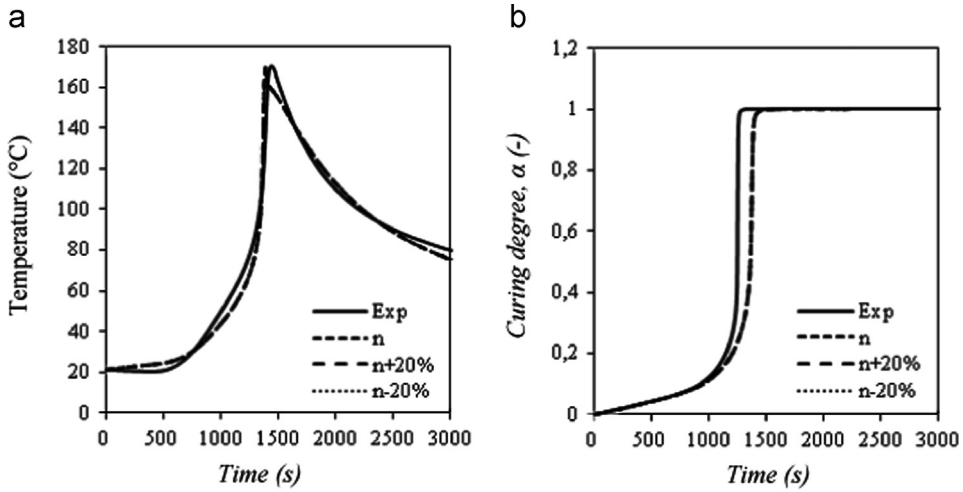

Fig. 19. Effect of the reaction order m on (a) the temperature-time history and on (b) the curing degree-time history at the point D (8;10) in the adhesive.

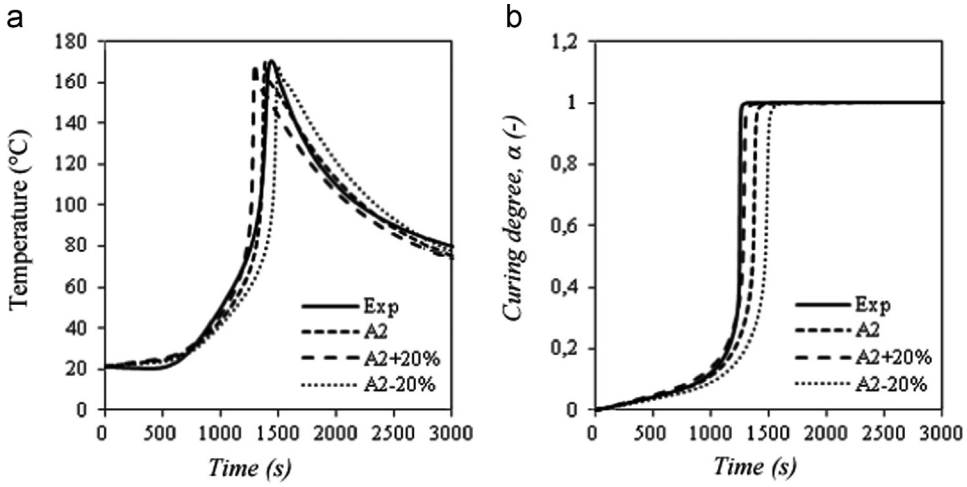

Fig. 20. Effect of the reaction order n on (a) the temperature-time history and on (b) the curing degree-time history at the point D (8;10) in the adhesive.

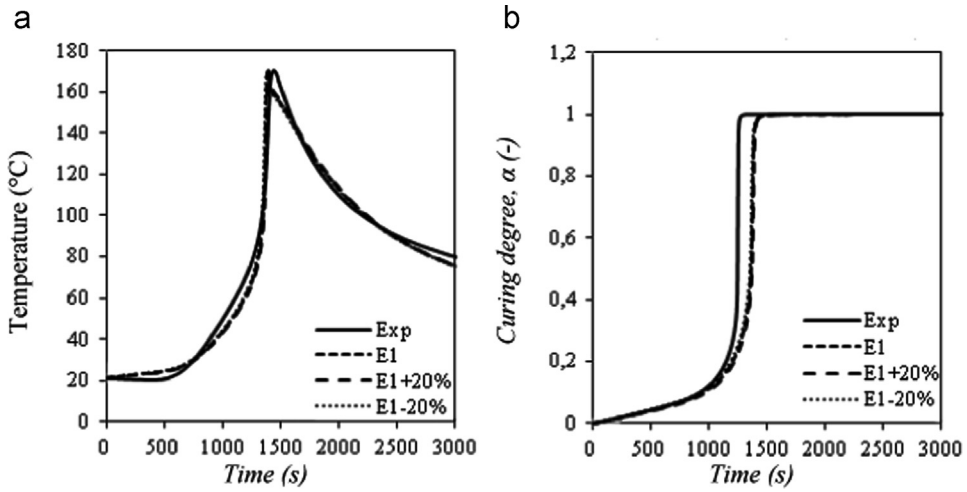

Fig. 21. Effect of the rate constant A_1 on (a) the temperature-time history and on (b) the curing degree-time history at the point D (8;10) in the adhesive.

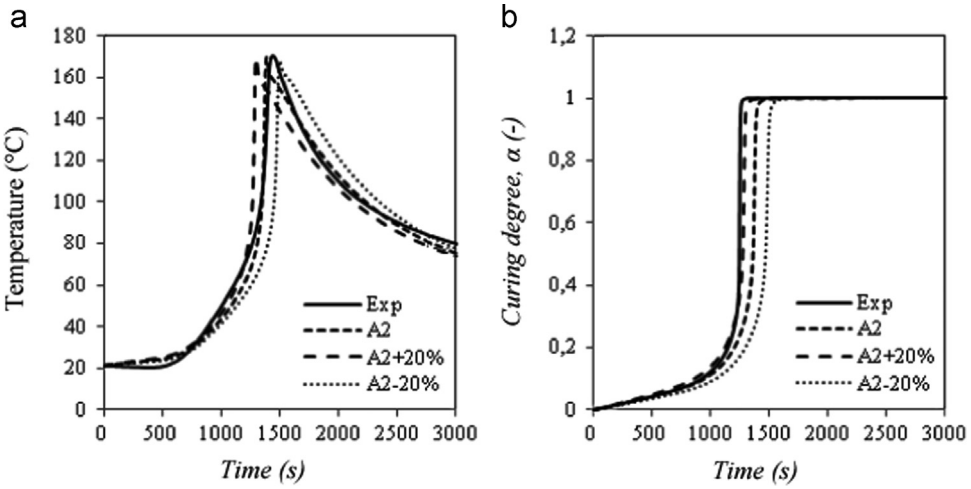

Fig. 22. Effect of the rate constant A_2 on (a) the temperature-time history and on (b) the curing degree-time history at the point D (8;10) in the adhesive.

Fig. 25 shows the influence of the thermal conductivity on the simulation responses. It appeared that thermal conductivity had negligible effects.

The specific heat affected the temperature-time and the curing degree-time histories (Fig. 26). It can be predicted, since, according to Eq. (1), the specific heat was related to the conduction heat and the internal heat generated from the cure. An increase in the specific heat caused a decrease in the maximum temperature reached and, therefore, delayed the time necessary to attain the maximum value of the curing degree: for Cp+20%, the maximum temperature was decreased by around 16 °C and the maximum curing degree was attained 235 s after the experiment.

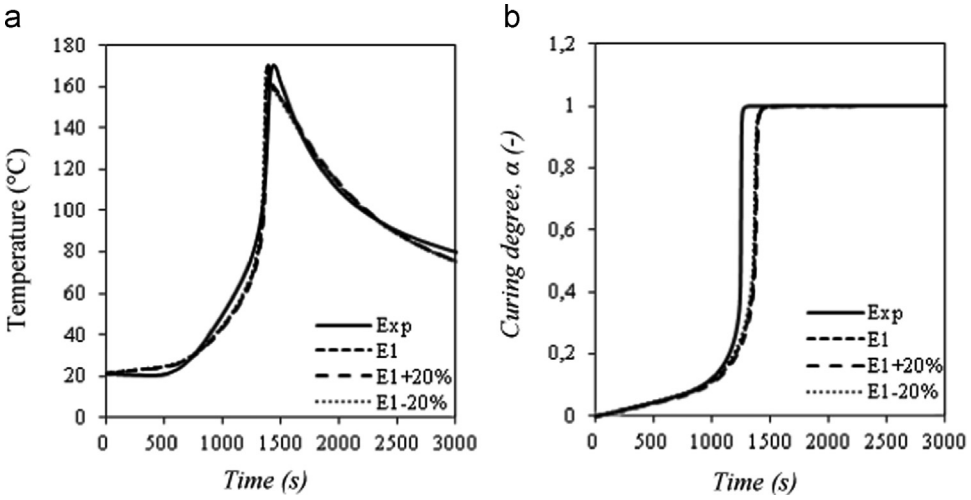

Fig. 23. Effect of the activation energy E_1 on (a) the temperature-time history and on (b) the curing degree-time history at the point D (8;10) in the adhesive.

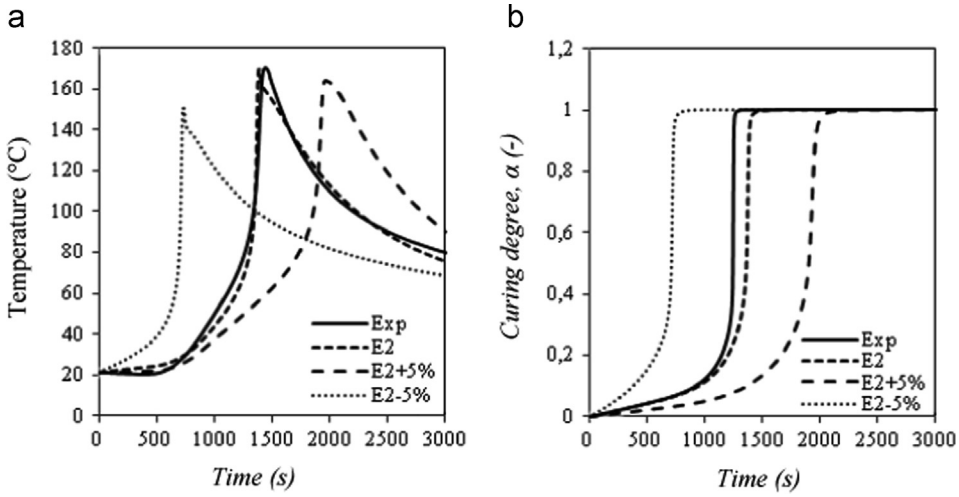

Fig. 24. Effect of the activation energy E_2 on (a) the temperature-time history and on (b) the curing degree-time history at the point D (8;10) in the adhesive.

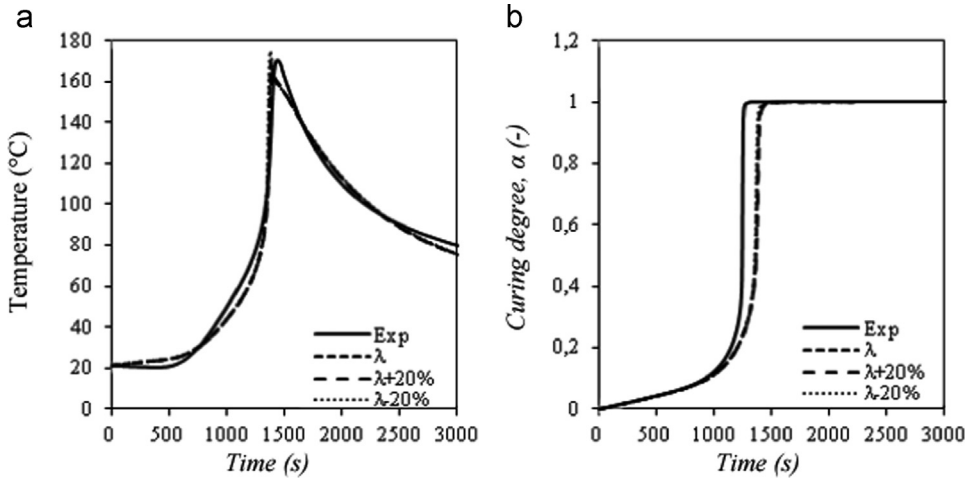

Fig. 25. Effect of the thermal conductivity on (a) the temperature-time history and on (b) the curing degree-time history at the point D (8;10) in the adhesive.

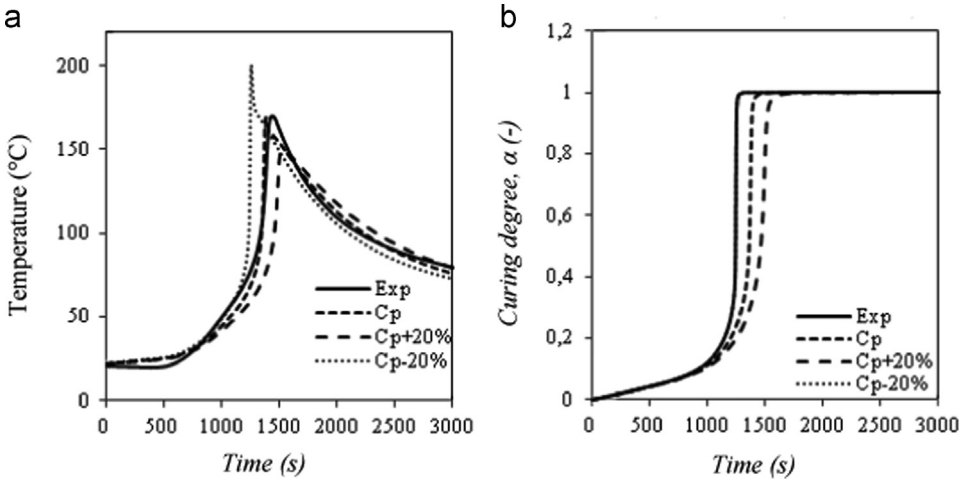

Fig. 26. Effect of the heat capacity on (a) the temperature-time history and on (b) the curing degree-time history at the point D (8;10) in the adhesive.

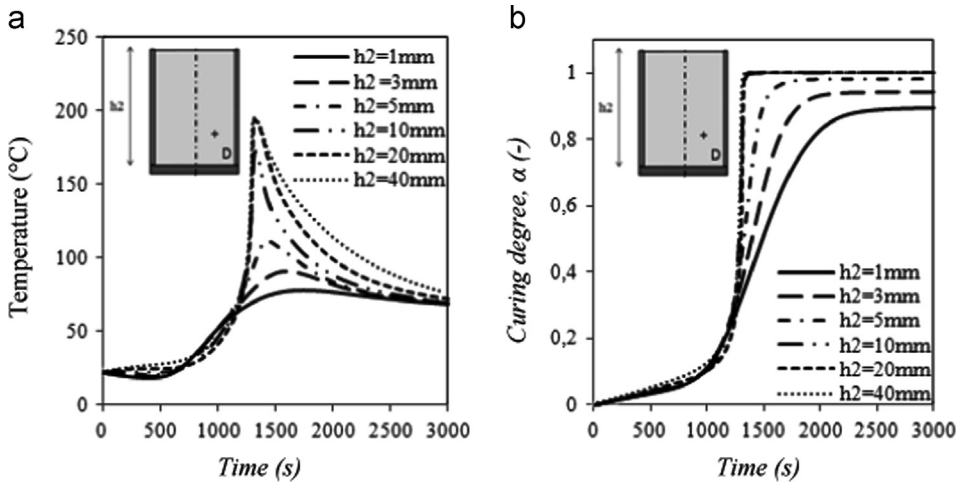

Fig. 27. Effect of the adhesive thickness on (a) the temperature-time history and (b) the curing degree-time history at the center of the adhesive.

As shown previously, thermal properties such as specific heat and thermal conductivity were described using a rule of mixture law. However, these material properties, particularly the specific heat capacity, have an influence on the temperature response predicted by the FEM model (Fig. 26). Fig. 14 shows a good correlation between experimental and numerical results. Therefore, it seems acceptable to use such laws.

3.4.5. *Thickness effects on cure predictions*

The effect of adhesive thickness on temperature and curing degree responses was studied. The simulation was based on the same boundary conditions and the same assumptions as previously. The temperature and the curing degree were taken at the center of the adhesive to reflect the thermal gradients generated during curing for several adhesive thicknesses.

Fig. 27 shows that the adhesive thickness generated thermal gradients during the curing of the adhesive. A decrease in the adhesive thickness caused a reduction in the maximum temperature reached at the center of the adhesive and, thus, a decrease in thermal gradients. The center of the adhesive was submitted to different curing cycles according to the adhesive thickness. Thus, the curing degree evolved differently as shown in Fig. 27(b). For instance, for a thickness of 1 mm, the maximum peak temperature was around 76 °C whereas this peak was of 194 °C for a thickness of 40 mm. It is not surprising that the maximum curing degree is lower for a thickness of 1 mm than for a higher thickness considering the thermal gradients generated during each curing cycle.

It appeared that parameters such as the total heat of the reaction, the specific heat, the rate constant A_2 and the activation energy E_2 played an important role in the curing process. Considering the influence on these parameters and the location of the thermocouples on the temperature-time and the curing degree-time histories, it can be concluded that the thermo-chemical model proposed accurately predicts the curing behavior of the adhesive Hysol EA-9321. Indeed, the discrepancies shown in Fig. 14 are negligible compared with those created by the sensitivity analysis.

4. Conclusions and perspectives

In this paper, the curing behavior of the adhesive Hysol EA-9321 was experimentally and analytically investigated. A thermo-kinetic model was used to study the temperature and curing degree distribution in an adhesive during curing process.

Regarding the curing kinetics of the adhesive, it can be concluded that:

– Autocatalytic model and isothermal Kamal and Sourour with diffusion models simulate the curing behavior of the adhesive Hysol EA-9321 well at low temperatures, i.e below the glass transition temperature. These models have to take into account

a heating rate-dependent pre-exponential factor and diffusion control.
- Curing the adhesive at low temperatures of 25–45 °C decelerates the curing process significantly. High curing degrees are obtained at higher temperatures of 80–100 °C and more rapidly.
- Concerning the potential use of this adhesive in the spatial domain, the long curing period at low temperatures provides curing degrees of around 50%. Hence, adhesive properties are subjected to change depending on the environment in which the adhesive evolves. Increasing curing temperatures or doing a post-cure are recommended in order to increase the curing state of the adhesive and thus to improve its properties.

The FE model was developed for a block of adhesive. The comparison with experimental data shows that the procedure is numerically stable and produces accurate results. This model makes the assumption that curing residual stresses (chemical shrinkage and thermal dilatation) are negligible.

The FE proposed is particularly interesting for applications for which large-scale bonded structures are used. These structures are generally erected and stored under outdoor conditions and the curing state of the bonded area is heterogeneous according to the thermal loadings applied, hence, the FE model used to indicate the curing degree at each location of the bonded area. Since the mechanical properties of the bonded assembly are curing degree dependent, it will be a way to predict the strength of the structure according to its curing state.

In future work, the determination of mechanical properties of the adhesive Hysol EA-9321 and their dependence on the curing state will be investigated. The knowledge of these properties will be a way to predict the lifetime of a bonded-structure.

References

[1] Henkel Hysol EA 9321, Technical data sheet.
[2] Huang HC, Usmani AS. Finite element analysis for heat transfer: theory and software. London: Springer; 1994. p. 13–4.
[3] Balvers J, Bersee H, Beukers A, Jansen K. Determination of cure dependent properties for curing simulation of thick-walled composites. In: Proceedings of the 49th AIAA/ASME/ASCE/AHS/ASC Structures, Structural Dynamics, and Materials Conference, Schaumburg, IL, USA, April 7–10; 2008.
[4] Johnston A. An integrated model of the development of process-induced deformation in autoclave processing of composite structures. Vancouver, B.C.: The University of British Columbia; 1997 [Ph.D. thesis].
[5] Gustafsson SE. The transient plane-source technique: for measurements of thermal conductivity and diffusivity of solid materials. Rev Sci Instrum 1991;62:797–804.
[6] Gustafsson SE. Thermal conductivity, thermal diffusivity, and specific heat of thin samples form transient measurements with hot disc sensors. Rev Sci Instrum 1994;65:3856–9.
[7] Van Mele B, Van Assche G, Van Hemelrijck A. Modulated differential scanning calorimetry to study reacting polymer system. J Reinf Plast Compos 1999;18 (No. 10).
[8] Skordos AA, Partridge K, Monitoring and Heat Transfer Modelling of the Cure of Thermoset Composites Processed by Resin Transfer Moulding, Polymer Composites'99, October 6–8, Canada, 1999.
[9] Chern B-C, Moon Tess J, Howell JR, Wiling Tan. New experimental data for enthalpy of reaction and temperature- and degree-of-cure-dependent. J Compos Mater 2002;36(17):2061–72.
[10] Bailleul J, Delaunay D, Jarny Y. Determination of temperature variable properties of composite materials: methodology and experimental results. J Reinf Plast Compos 1996;15:479–96.
[11] Mijović J, Wang HT. Modeling of Processing of Composites Part II—Temperature Distribution during Cure. SAMPE J 1988;191:42–55.
[12] Moisala A, Li Q, Kinloch IA, Windle AH. Thermal and electrical conductivity of single- and multi-walled carbon nanotube-epoxy composites. Compos Sci Technol 2006;66:1285–8.
[13] H QUOTE hne GWH, Hemminger WF, Flammershein HJ. Differential scanning calorimetry. New York: Springer Verlag Berlin Heidelberg; 2003.
[14] Zhang Y, Adams RD, F.M. da Silva Lucas. Effects of curing cycle and thermal history on the glass transition temperature of adhesives. J Adhes 2014;90:327–45.
[15] Mettler Toledo,⟨www.mt.com⟩, Viroflay, France.
[16] Liljedahl CDM, Crocombe AD, Abdel Wahab MM, Ashcroft IA. The effect of residual strains on the progressive damage modelling of environmentally degraded adhesive joints. J Adhes Sci Technol 2005;19(7):525–47.
[17] Zvetkov Valery L. Thermochim Acta 2005;435:71.
[18] Lee JY, Choi HK, Shim MJ, Kim SW. Kinetics studies of an epoxy cure reaction by isothermal DSC analysis. Thermochim Acta 2000;343(1–2):111–7.
[19] Yousefi A, Lafleur PG, Gauvin R. Kinetic studies of thermoset cure reactions: a review. Polym Compos 1997;18(2):157–68.
[20] Arrhenius. Über die Dissociationswärme und den Einfluss der Temperature auf den Dissociationsgrad der Elektrolyte. Z Phys Chem 1989;4:96–116.
[21] Sun L, Pang S, Sterling A, Negulescu I, Stubblefield M. Thermal analysis of curing process of Epoxy Prepreg. J Appl Polym Sci 2002;83(5):1074–83.
[22] Sun L, Pang S, Sterling A, Negulescu I, Stubblefield M. Dynamic analysis of curing process of Epoxy Prepreg. J Appl Polym Sci 2002;86(8):1911–23.
[23] Kissinger HE. Reaction kinetics in differential thermal analysis. Anal Chem 1957;29:1702–7.
[24] Moré JJ. The Levenberg–Marquardt algorithm: implementation and theory, numerical analysis. In: Watson GA, editor. Lecture notes in mathematics. Springer Verlag; 1977. p. 105–16 630.
[25] Cartwright JHE, Piro O. The dynamics of Runge–Kutta methods. Int J Bifurc Chaos 1992;2:427–49.
[26] Horie K, Hiura H, Sawada M, Mita I, Kambe H. Calorimetric investigation of polymerization reactions III. Curing reaction of epoxides with amines. J Polym Sci: A-1 1970;8:1357–72.
[27] Kamal MR, Sourour S. Kinetics and thermal characterization of thermoset cure. Polym Eng Sci 1973;13(1):59–64.
[28] Kamal MR, Sourour S. Differential scanning calorimetry of epoxy cure: isothermal cure kinetics. Thermochim Acta 1976;14:41–59.
[29] Chern CS, Phoehlein GW. A kinetic model for curing reactions of epoxides with amines. Polym Eng Sci 1987;27:788–95.
[30] ASTM E 1269, Standard test method for determining specific heat capacity by differential scanning calorimetry; 2005.
[31] Yu H, Adams RD, da Silva Lucas FM. Development of a dilatometer and measurement of the shrinkage behavior of adhesives during cure. Int J Adhes Adhes 2013;47:26–34.